Mg/Ca in fossil oyster shells as palaeotemperature proxy, an example from the Palaeogene of Central Asia

Laurie Bougeois, Marc De Rafélis, Gert-Jan Reichart, Lennart De Nooijer, Guillaume Dupont-Nivet

Mg/Ca in fossil oyster shells as palaeotemperature proxy, an example from the Palaeogene of Central Asia.

Laurie Bougeois[a,b,*], Marc de Rafélis[a,c], Gert-Jan Reichart[d,e], Lennart J. de Nooijer[e], Guillaume Dupont-Nivet[b,d,f,g]

[a] *ISTeP, UMR 7193, Université Pierre et Marie Curie, Paris, France*
[b] *Géosciences Rennes, UMR-CNRS 6118, Université de Rennes 1, Rennes, France*
[c] *GET, Observatoire Midi Pyrénées, Université de Toulouse, CNRS, IRD, Toulouse, France*
[d] *Department of Earth Sciences, Utrecht University, Utrecht, The Netherlands*
[e] *Department of Geology and Chemical Oceanography, Royal Netherlands Institute for Sea Research, Texel, The Netherlands*
[f] *Department of Earth and Environmental Sciences, Potsdam University, Germany*
[g] *Key Laboratory of Orogenic Belts and Crustal Evolution, Ministry of Education, Beijing, China*

Abstract

Fossil oyster shells are well-suited to provide palaeotemperature proxies from geologic to seasonal timescales due to their ubiquitous occurrence from Triassic to Quaternary sediments, the seasonal nature of their shell growth and their strong resistance to post-mortem alteration. However, the common use to translate calcitic oxygen isotopes into palaeotemperatures is challenged by uncertainties in accounting for past seawater $\delta^{18}O$, especially in shallow coastal environment where oysters calcify. In principle, the Mg/Ca ratio in oyster shells can provide an alternative palaeothermometer. Several studies provided temperature calibrations for this potential proxy based on modern species, nevertheless their application to palaeo-studies remains hitherto unexplored. Here, we show that past temperature variability in seawater can be obtained from Mg/Ca analyses from selected oyster fossil species and specimens. High-resolution Mg/Ca profiles, combined with $\delta^{18}O$, were obtained along 41 fossil oyster shells of seven different species from the Palaeogene Proto-Paratethys sea (Central Asia) found in similar as well as different depositional age and environments providing comparison. Suitable Mg/Ca profiles, defined by continuous cyclicity and reproducibility within one shell, are found to be consistent for specimens of the same species but differ systematically between species, implying a dominant species-specific effect on the Mg/Ca incorporation. Two species studied here (*Ostrea (Turkostrea)* strictiplicata and *Sokolowia buhsii*) provide an excellent proxy

*Corresponding author at: ISTeP, Université Pierre et Marie Curie, 4, place Jussieu 75005 Paris, France.
Email address: laurie.bougeois@gmail.com (Laurie Bougeois)

for palaeoclimate reconstruction from China to Europe in Palaeogene marine sediments. More generally, the protocol developed here can be applied to identify other fossil oyster species suitable for palaeoclimate reconstructions.

Keywords: palaeoclimate, oyster, Mg/Ca, sclerochronology, Palaeogene, Central Asia

1. Introduction

The ability to track quantitatively climate seasonality patterns through the geological record is key to understand past, present and future climate processes (Felis et al., 2004; Licht et al., 2014). However, most palaeoclimate proxies yield only qualitative assessments of seasonality or insufficient resolution averaging across thousands of years (Eldrett et al., 2007; Evans et al., 2013).

In contrast, bivalve shells have long been recognized to potentially represent excellent high-resolution (i.e. infra-annual) palaeoclimate archives (e.g. Hudson et al., 1976; Richardson, 2001). The shell of bivalves is formed by incremental growth resulting in a record that can be sampled at an intra-annual resolution (Stenzel, 1971; Kirby et al., 1998). Moreover, they live over a large range of climate regimes and habitats (Surge et al., 2001; Mouchi et al., 2013). In addition, their generally large and thick calcitic shells promote good preservation of fossils such that oysters represent one the most abundant macro-fossil groups readily available in the sedimentary records (Stenzel, 1971).

When biomineralizing, bivalve species have been shown to build their shell in isotopic equilibrium with sea water and therefore, its stable oxygen isotope ratios ($\delta^{18}O$) reflect seawater temperatures in which the organisms formed its shell (Killingley and Berger, 1979; Wefer and Berger, 1991; Ivany et al., 2000). However, carbonate $\delta^{18}O$ also varies with the stable oxygen isotopic composition of seawater ($\delta^{18}O_{sw}$, e.g. Anderson and Arthur, 1983), such that measured isotope ratios corresponds to a combination of past seawater temperature and isotope composition. Estimating seawater isotopic composition and its intra-annual variability in the geologic past remains a major challenge to isolate the temperature signal from shell oxygen isotopes. In principle, seawater oxygen isotope composition can be resolved using a second independent temperature proxy, not primarily depending on salinity or seawater oxygen isotope composition. Such a proxy may be available from minor and trace elements in biominerals, particularly the Mg/Ca and Sr/Ca ratios in carbonates are known to reflect past seawater temperatures in foraminifera (e.g. Nürnberg et al., 1996; Lear et al., 2000) and corals (Lough, 2010), respectively. Based on Mg/Ca and Sr/Ca, these temperatures can be

combined with carbonate $\delta^{18}O$ to estimate past seawater $\delta^{18}O$, which in turn reflects seawater salinity (Elderfield and Ganssen, 2000; Lear et al., 2000; Bougeois et al., 2014).

Accurate minor/trace element-temperature calibration for bivalve shells have long been unavailable by a lack of appropriate controlled growth studies (Dodd, 1965). More recently, many studies succeeded in relating seawater temperature to bivalve calcitic Mg/Ca ratio in mussels (Klein et al., 1996; Vander Putten et al., 2000; Freitas et al., 2009; Wanamaker et al., 2008), scallop (Freitas et al., 2006, 2009, 2012), fan mussels (Freitas et al., 2005), and oysters (Surge and Lohmann, 2008; Mouchi et al., 2013). These studies revealed relatively large inter-specific differences in temperature sensitivity (see Table 1 for different calibrations). In addition, environmental conditions exert a strong impact on bivalve Mg/Ca even within one species. For example, calibrations differ for *M. edulis* when calcifying in estuarine, culture or natural brackish waters (eq. 6, 7 and 8 in Table 1), suggesting that variables other than temperature additionally determine bivalve calcite chemistry (Freitas et al., 2005, 2006, 2009, 2012). These suggested variables include metabolism (Rosenberg and Hughes, 1991; Vander Putten et al., 2000), intra-shell variability (Freitas et al., 2009), salinity and growth rate (Wanamaker et al., 2008) on *Mytilus edulis*. Studies also revealed an ontogeny-related effect in *Pinna nobilis* (Freitas et al., 2005) and an impact of incorporated organic matter (mainly conchiolin) on bivalve aragonite shell chemistry in *Arctica islandica* (Schöne et al., 2010). These effects are negligible in oyster shells in which incorporation of organic compounds into the carbonate crystal lattice, especially in foliated calcite, is much lower than in other bivalve (e.g. mussels and scallops; Stenzel, 1971). Furthermore, the oyster's conchiolin is relatively easily degraded by bacterial activity, so that even the organic content of older parts of the shell has already decreased during the life of the animal and is absent in fossil oysters (Stenzel, 1971). Recent studies also showed that impacts of salinity, ontogeny and growth rate are modest compared to that of temperature on Mg incorporation into the foliated oyster calcite shell (Surge and Lohmann, 2008; Mouchi et al., 2013). Furthermore, duplicate of Mg/Ca ratio analyses in the ligamental area showed that intra-shell small scale variability for magnesium is negligible (Bougeois et al., 2014).

Although these considerations clearly designate oyster shells as prime targets for palaeoclimate reconstructions using Mg/Ca, such analyses have yet to be tested using a thorough analytical protocol. We previously conducted a pilot study on a single fossil oyster shell (*Sokolowia buhsii*) from the Eocene Proto-Paratethys sea in Central Asia suggesting that its Mg/Ca may be used to recon-

struct palaeotemperatures (Bougeois et al., 2014). However, to constrain the reliability of Mg/Ca as a palaeothermometer for the geological past and to quantify inter-specimen variability in element composition, additional investigations on specimens and species from a range of environments and ages are necessary. Here, we extend the approach to various Palaeogene oyster species including different environmental and stratigraphic contexts well-constrained by parallel studies of the western Proto-Paratethys sea (Bosboom et al., 2014a,b,c) (Bosboom et al., 2014a,b,c). We aim to determine whether Mg/Ca ratios yield reliable and reproducible environmental intra-annual proxy data in fossil oyster shells from various species and environments and thereby the reliability of the Mg/Ca-temperature calibration established on modern oysters when applied to fossil specimens.

2. Context of sampling

2.1. Environmental and stratigraphic setting

During Palaeogene times, a large shallow epicontinental sea belonging to the Tethyan Realm covered the Eurasian continent from the Mediterranean Tethys (west side) to the Tarim Basin (western China, east side) (Dercourt et al., 1993; Burtman, 2000). In the Tarim Basin (Xinjiang, China), the Afghan-Tajik depression (Afghanistan-Tajikistan), the Fergana basin and the Alai Valley (Kyrgyzstan) (Figure 1a, b), regional regression-transgression sequences have been established based on inter- and intra- basin stratigraphic correlations of the deposits with distinct lithological facies and fossil assemblages including bivalves, dinoflagellate cysts, foraminifera and ostracods (see Bosboom et al., 2014a,b,c, and references therein). From the Cenomanian to the final sea-retreat dated late Bartonian–early Priabonian, five major second-order marine incursions have been recognized in the sedimentary record in Central Asia. The marine intervals are dominated by bioclastic wackestones to grainstones, evaporites, clay and mudstones containing ostracods, gastropods, bryozoa, serpulids, echinoids, foraminiferas, algae, fish scales and molluscs. Bivalve calcitic shells such as Ostreidae and Pectinidae mainly remained in sedimentary deposits, whereas aragonite molluscs were leached and not preserved. Sedimentary facies and fossils assemblages are characteristic of shallow coastal environments between offshore to coastal plains, and typical of a carbonate-rich neritic ramp (Manceau et al., 2014).. Continental intervals between marine incursions contain fine to middle grained detrital rocks, red clay to siltstones and evaporitic deposits characterised by nodular and massive gypsum. These deposits are indicative of flood plains, alluvial plains and playa environments. Sedimentary

deposits indicate alternation between more humid and dry periods, typical of semi-arid climates with a relatively strong seasonal contrast (Manceau et al., 2014).

2.2. Oyster sampling, age and determination

Mollusc macrofauna taxonomic identification largely follows Lan and Wei (1995), Lan (1997) and Bosboom et al. (2014a,c), representing the most recent revision of regional systematic literature. Fossil ages were estimated using mollusc biostratigraphy (Lan and Wei, 1995) and adjusted for the two last marine incursions from recent studies combining bio- and magnetostratigraphy in this region (Bosboom et al., 2014a,b) (Figure 1c). Specimens from the oyster species *Ostrea bellovacina* (Late palaeocene, Thanetian), *Flemingostrea hemiglobosa* (Early Eocene, Ypresian), *Sokolowia orientalis* (Middle Eocene, Early Lutetian), *Ostrea (Turkostrea) strictiplicata* (Middle Eocene, Early to Middle Lutetian), *Sokolowia buhsii* (Middle Eocene, Middle to Late Lutetian), *Platygena asiatica* (Middle Eocene, Late Bartonian) and *Ferganea bashibulakeensis* (Middle Eocene, Early Priabonian) were extracted from marine sediment strata in Central Asia during field excursions in the summers of 2007, 2010, 2011, 2012 and 2013 (Figure 1). All taxa belong to the Superfamily Ostreaoidea and the Families Ostreidae or Flemingostreidae (Carter et al., 2011). Specimens were selected according to the following criteria: (1) good preservation of the shell, particularly of the ligamental area, (2) sufficiently large ligamental surface to contain growth bands spanning more than ten years and providing a high resolution, (3) specimens fossilized in living position attesting of the living environment. Field sedimentological analyses yield characterisation of the depositional environmental for each species (Figure 2, Manceau et al., 2014).

3. Material and methods

To determine the applicability of Mg/Ca as a temperature proxy we have combined a number of analyses on specimens from different species and representative of a range of environments. To detect potential diagenetic alteration and identify the presence of seasonal banding, shells were first analysed with cathodoluminescence microscopy. Trace element analyses were then performed at high resolution yielding Mg/Ca variations with varying reliability criteria defined below. Finally, to provide a reference for comparing and assessing the Mg/Ca results, stable isotope analyses were also performed at high incremental resolution and/or on bulk samples (Table 2).

3.1. Shell description and sample preparation

Oyster shells grow by incremental deposition of calcium carbonate (mainly calcite), resulting in alternating dark and light bands corresponding to the colder and warmer seasons respectively (Kirby et al., 1998). The foliated calcite forming the ligamental area (or umbo) is very dense and resistant to post-mortem alteration, resulting in conservation of the primary environmental signal. For this reason, we focused our chemical analyses to the ligamental area, following practice from a number of previous studies (Kirby et al., 1998; Surge and Lohmann, 2008; Lartaud et al., 2010b; Goodwin et al., 2012; Mouchi et al., 2013; Bougeois et al., 2014).

After isolation from the sediment and thorough cleaning of the shell's surface by brushing off loose material and rinsing with deionized water, specimens were prepared for sclerochronological and geochemical analysis by cutting 0.5 cm-thick slices along the maximum growth axis of the left valve in the middle of the resilifer (Figure 3). These sections were subsequently polished and cleaned in an ultrasonic bath with deionized water for ten minutes and dried overnight. Radial sections reveal numerous growth lines providing a continuous record along the oyster's lifetime (Figure 3). Shell slices were then sectioned into slices of maximum 2.5 cm width and 5.0 cm length to fit the sample holder for geochemical analyses.

3.2. Cathodoluminescence analyses

Shell preservation and potential impact of diagenesis are commonly detected in bivalve shells using cathodoluminescence (CL) microscopy (e.g. Langlet et al., 2006). In calcite, Mn^{2+} is the main luminescence activator, causing emission of yellow to orange light of which the intensity is positively correlated with Mn concentration (El Ali et al., 1993; De Rafélis et al., 2000; Habermann, 2002; Langlet et al., 2006). As Mn is also preferentially incorporated in the oyster shell calcite during summer months (Langlet et al., 2006; Lartaud et al., 2010b), this results in high luminescence intensities during summer and conversely relatively low luminescence during winter. Thus variations of the CL intensity following the shell's growth axis in each slab and can thus be used as a rapid and non-invasive method to identify the presence of seasonal banding (Bougeois et al., 2014). CL analyses were performed at the Université Pierre et Marie Curie (Paris, France) on a cold cathode device (Cathodyne OPEA) coupled to an optical microscope and a digital camera.

3.3. Trace element analyses

Trace element composition was determined by Laser Ablation-Inductively Coupled-Plasma-Mass Spectrometry (LA-ICP-MS), with a Geolas 200Q Excimer 193 nm laser coupled to a sector field ICP-MS (Element2, Thermo Scientific) at the Utrecht University (The Netherlands). The sectioned oyster shells were ablated at lower energy density ($\sim$1 J.cm^{-2}) by moving the sample in x, y, and z axis at a constant speed underneath the laser beam in a He environment. The path was programmed so that subsequent circular ablation spots (120 µm in diameter) overlapped slightly and resulted in a resolution of one data point every $\sim$7 µm leading in more than 100 measurements for each growth band. All transects were ablated perpendicularly to the growth axis to monitor consistency of obtained profiles. To test data consistency and quantify intra-shell variability inside the umbo, each transect was duplicated by a second parallel transect spaced at approximately 0.5 to 1 mm from the first one. Masses monitored by the ICP-MS included ^{24}Mg, ^{26}Mg, ^{43}Ca, ^{44}Ca,^{55}Mn, ^{88}Sr and ^{138}Ba, using the international standard NIST SRM610 (using element concentrations reported in Jochum et al., 2011) and ^{43}Ca as an internal standard (assuming 40% wt in $CaCO_3$). The glass standard was ablated between measurements of each oyster at a higher energy density ($\sim$5 J.cm^{-2}). Calibration of element/calcium ratios in calcium carbonate samples was obtained with the NIST glass standard yielding accurate values for many elements when using a 193 nm laser as indicated by similar fractionation factors obtained when using glass and carbonate standard material, despite differences in ablation characteristics for these materials (Hathorne et al., 2008). Here, we mainly focus on the obtained patterns in Mg/Ca (for more details about the LA-ICP-MS protocol, see Bougeois et al., 2014). To account for small scale fluctuations in the Mg/Ca ratio, corresponding values from the two parallel transects were averaged so that a single data-point was obtained for each incremental position. On these data-points, a moving average using a Bartlett window was then run through data from every transect as previously described in (Bougeois et al., 2014).

3.4. Stable isotopes analyses

Stable oxygen isotopes were analysed (1) at high incremental resolution aiming to resolve seasonal variability and (2) on bulk samples aiming to average the isotopic record throughout the oyster's life. Bulk carbon isotopes (δ^{13}C) were also analysed to assess potential environmental effects on the shell's chemistry. To collect material for these analyses, a high-precision, computer-driven Micromill (New Wave Research) attached to an x, y and z stage was used to follow digitized

milling path positions. Bulk analyses were performed by milling one continuous line following laser transects across the ligamental area. For incremental analyses, parallel paths were milled every 100-120 μm following the growth bands (Figure 3). At least 30 to 50 μg of calcitic shell powder was collected for each milled sample and analysed for oxygen and carbon stable isotopes ($\delta^{18}O$ and $\delta^{13}C$ in ‰ VPDB) using a KIEL-III device coupled online to a Finnigan MAT-253 mass spectrometer at Utrecht University for incrementally resolved data of the specimens AT11-O04, KZ07-O01, KY10-O01. Material from all other specimens and for bulk analyses were analysed using a KIEL-IV carbonate device at the Université Pierre et Marie Curie (UPMC, Paris, France). The international standard NBS-19 and an in-house standard (Naxos marble in Utrecht University and Marceau in UPMC) were used for calibration of all sample sets. For both instruments, long-term analytical precision was better than 0.08‰ for $\delta^{18}O$ and better than 0.05‰ for $\delta^{13}C$.

For the oysters analysed at the Utrecht University the entire length of each shell specimen was milled for incremental study at high resolution (one sample every 120 μm) totalling ∼130 samples per shell for ∼20 cycles (or years). Results from this first batch of samples indicate that a slightly lower resolution was sufficient except for intervals with much lower growth rates (and thus thinner bands). This justified a drilling resolution of only 5 to 8 annual cycles into the remaining specimens that all displayed higher growth rates and thereby enabled increasing the total number of specimens analysed. At a resolution of one micro-milled sample every 100 to 200 μm (samples with sufficiently high growth rates were analysed with only one micro-sample every 200 μm) between 42 and 82 samples were thus analysed per specimen. This enabled the incremental stable isotope analyses for 20 carefully-chosen shells (out of the 41 shells initially analysed for trace element composition) while bulk stable isotope analyses was performed on 40 shells, to obtain at least one stable isotopic value for each specimen.

4. Analytical results

4.1. Cathodoluminescence results

In total, 38 oyster shells were analysed with cathodoluminescence microscopy. In general, clear and consistent banding in CL intensities show that diagenetic effects potentially affecting the analysed oyster shells were minimal, indicating a good preservation of the carbonaceous skeleton. A cyclic pattern is well defined for the species *S. buhsii*, *O. (T.) strictiplicata* and *O. bellovacina* with

alternations between intense luminescence for the light summer bands and lower luminescence intensities for the dark winter growth bands. The luminescence for *F. hemiglobosa* is very weak and the luminescence for *F. bashibulakeensis* is inverted with thinnest layers corresponding to winter growth deceleration (Richardson et al., 1993; Kirby, 2001) with relatively bright luminescence (Figure 3).

4.2. Trace element results

A total of 41 shells were analysed for trace elements. Mg/Ca values range between 1.06 and 14.33 mmol/mol. Average Mg/Ca values for a single specimen varies from 2.74 to 9.75 mmol/mol (Figures 6 7, 8 and 9e-h).

The intra-shell patterns in Mg/Ca vary between specimens and we therefore evaluated the quality of the results using two properties: (1) the small-scale intra-shell variability, which is the difference between patterns in Mg/Ca from the two parallel transects; (2) the cyclicity in Mg/Ca reflecting whether a primary seasonal signal has been recorded. According to these criteria we grouped the Mg/Ca results into three categories (Table 2):

- suitable (continuously cyclic and consistent between parallel transects, Figure 6)
- partly suitable (only some parts are cyclic and consistent between transects, Figure 7)
- unsuitable (non cyclic and/or not consistent between parallel transects, Figure 8).

For example Mg/Ca ratios from specimen KZ12-O05.1 (Figure 8) display a cyclic pattern but the absolute values of the two transects are clearly different and therefore this sample is qualified as unsuitable. Transects from the specimen MS12-O06.5 (Figure 7) display very consistent values from 7 to 19 cm but not from 0 to 7 cm, therefore it is qualified as partly suitable. These reliability assessments based on elemental results provide a useful criterion for selecting promising specimen before engaging into further isotopic analyses. Unsuitable specimens were discarded altogether from further isotopic analyses. In suitable and partly suitable specimens, well-defined continuous parts were selected for further isotopic analyses. Of all shells analysed (n=41), 12 were considered suitable, 13 partly suitable and 16 unsuitable (Table 2).

4.3. Stable isotopes results

All isotopes values obtained (bulk sample analyses and high-resolution incremental analyses) range between -5.45‰ and -0.57‰ for $\delta^{18}O$ and between -0.74‰ and 2.53‰ for $\delta^{13}C$ (Figure

5). For each sample, the average value derived from averaging all incremental analyses compares well with values from the bulk sample analyses (Figure 9a-d and Supplementary data). Specimens retrieved from the same stratigraphic bed usually exhibit similar values - standard deviation within 0.3‰ for $\delta^{13}C$ and 0.4‰ for $\delta^{18}O$- indicating homogeneous isotope ratios in oyster shells living at the same time and in a similar environment.

The well-resolved cyclicity observed in the oyster's isotopes confirms that sampling resolution (every 100-200 µm; depending on growth rates) was sufficiently high to clearly reveal intra-annual environmental variations with regular cyclicity. However, on two samples with particularly low growth rates in the oldest part of the shell (AT11-O04 and KY10-O01, Figure 5) the expression of seasonality is poor. This most likely results from a sampling bias, mixing material between closely spaced adjacent growth bands rather than an ontogenetic effect or a change in environmental variations or as previously shown in (Bougeois et al., 2014). We therefore discarded these parts of the shell record from further consideration.

5. Discussion

In light of the obtained analytical results, we discuss below (1) the reliability of Mg/Ca records in the various shell species analysed (2) species and environmental effects and (3) the validity of proposed calibrations of the Mg/Ca as a proxy for temperature for various species and depositional environments.

5.1. Reliability of Mg/Ca profiles for different species

It appears that reliability of Mg/Ca records varies between species and the species-specific patterns in Mg/Ca are therefore discussed separately.

- *O. (T.) strictiplicata* and *S. buhsii* mostly yield suitable and some partly suitable Mg/Ca data (Figures 6 and 7, Table 2). Variations are cyclic and correlate well with the other geochemical proxy $\delta^{18}O$. No clear ontogenetic effect can be recognized for the Mg incorporation in oyster shells, and CL indicates that diagenesis did not affect the shells analysed here. Furthermore, for specimens with both bulk and incremental stable isotope data, the bulk values compare well with the average of all the incremental $\delta^{18}O$ values within 0.4±0.2‰ (see Figure 9a-d). This underlines the homogeneity of the isotopic composition within the ligamental area

and further excludes that ontogeny has a large effect on oyster stable isotope ratios. The stable isotope values display a well-defined cyclicity with low values coinciding with light bands and high $\delta^{18}O$ corresponding to darker bands (Figures 4 and 5) revealed by CL. This is in agreement with previous observations showing a seasonal isotopic signal corresponding to variation of the CL intensity (Lartaud et al., 2010b; Bougeois et al., 2014). Similarly, stable isotope values are correlated to the suitable and partly suitable Mg/Ca results with low $\delta^{18}O$ values coinciding with highest Mg/Ca values as shown in Figure 4. Considering that in modern oyster shells Mg/Ca covaries with temperature (Surge and Lohmann, 2008; Mouchi et al., 2013), CL intensity increases during summer months (Langlet et al., 2006; Lartaud et al., 2010b) and $\delta^{18}O$ is negatively correlated to temperature (Anderson and Arthur, 1983), we conclude that all the geochemical tracer analysed in the fossil shells selected here reflect a primary environmental signal. Moreover, the results from these species are all cyclic suggesting seasonal variations in conditions which makes Mg/Ca (and $\delta^{18}O$) a promising tool for intra-annual palaeoclimate reconstructions.

- *F. bashibulakeensis* specimens yielded no suitable profiles, a few partly suitable and mainly unsuitable results displaying a non-cyclic pattern with highly variable Mg/Ca ratios throughout the shell. This may be partly explained by the curvature of the ligamental area affecting the reliability of the positioning of the sampling transects. This is supported by the fact that parts of the transects that may be suitable are perpendicular to the growth direction while unsuitable part of the transects cross the growth bands at an oblique angle. We therefore conclude that species with a curved ligamental area are less suitable for trace element analyses as performed here. Developing a new sampling method following the curvature more closely may yield more reliable results in oysters with strongly curved ligamental areas.

- *F. hemiglobosa* and *O. bellovacina* yielded no suitable profiles, a few partly suitable and many unsuitable Mg/Ca patterns characterized by variable intra-shell composition and absence of a well-defined cyclicity (Figure 8). This was observed even from samples from the same stratigraphic level in the Kuhdara section suggesting this is not an actual environmental effect (Table 2). In addition, this unreliability is unlikely caused by diagenesis, since the incremental $\delta^{18}O$ data of these shells display regular cycles (Figure Figure 5) and that CL values show no alteration through the ligamental area indicating good preservation. For some

specimens of *F. hemiglobosa*, the apparent mismatch in cyclicity between the stable isotopes and Mg/Ca, may be caused by the position of the cutting plane, which crossed the side of the ligamental area (within a side bead along the resilifer) instead of cutting through the middle. Considering the very low CL intensity (partially correlated to Mn concentration) and the unsuitable Mg/Ca signal, trace element incorporation appear to be altered in the side parts of the ligamental area, making them unsuitable for application of trace elements to environmental reconstructions. However, this can not explain all unsuitable data. A few other *F. hemiglobosa* and *O. bellovacina* present substantial intra-shell variability in Mg/Ca (e.g. MS13-O23, KZ12-O12.2 or Kuhdara samples, Table 2) although they have been cut properly and CL as well as $\delta^{18}O$ show cyclic variations with no diagenetic overprint. The cause of the mismatch between $\delta^{18}O$ and Mg/Ca remains to be investigated for these Palaeocene species. The non-cyclic pattern of trace element incorporation may relate to species-specific or environmental effects and are discussed below.

5.2. Environmental and species effects

Oyster shells from the same sedimentary level (that have calcified at the same time and location) yielded similar isotopic and Mg/Ca records (Figure 9j). However, these values differ significantly and sometimes systematically when comparing different species, time periods and/or living environments suggesting that the records depend both on species and on environmental conditions. Comparison of the $\delta^{13}C$ and $\delta^{18}O$ from bulk and incremental average data (Figure 9i) shows that the samples can be divided into two groups: one with both depleted $\delta^{18}O$ and $\delta^{13}C$ values and one with more enriched $\delta^{18}O$ and $\delta^{13}C$ values. This may reflect the influence of freshwater (by e.g. continental runoff), resulting in depleted carbon and oxygen isotope rations of shell for species living in the shallowest sites (Lartaud et al., 2010a). This is particularly clear when comparing values from the species *F. hemiglobosa* in offshore environments at the Aertashi section to values from the same species in a relatively nearshore bay environment at the Mine and Kuhdara sections (Figure 9i). Furthermore, *O. (T.) strictiplicata*, *S. orientalis* and *S. buhsii* are all collected from fully subtidal marine environments and have similar $\delta^{18}O$ and $\delta^{13}C$ to other fully marine specimens and differ strongly from, for example, *P. asiatica* that lives in a nearshore mangrove environment (Figure 2). Despite this apparent systematic environmental effect on isotopic fractionation, it remains to be investigated whether this is also reflected in the Mg/Ca since reliable profiles (i.e. suitable and

316 reliable parts of partly suitable profiles) were not available from specimens of the same species that
317 calcified in different depositional environments. Only *F. hemiglobosa* provides this opportunity, and
318 shows no significant differences between specimens collected from various environments as most
319 analyses are unsuitable.

320 To estimate potential species-specific effects, multiple reliable Mg/Ca profiles are compared from
321 different species from the same living environments (Figure 9). Mg/Ca results within a species col-
322 lected from one area and the same geological period are relatively similar (based on the standard de-
323 viation of their average Mg/Ca). This indicates consistency of the Mg/Ca signal between specimens
324 of one single oyster species. However, absolute values and the range of Mg/Ca ratio vary between
325 species. For instance, *O. (T.) strictiplicata* and *S. buhsii* (Middle Eocene) have Mg/Ca averages of
326 approximately 6 mmol/mol with a seasonal amplitude of ∼5 mmol/mol. For *F. hemiglobosa* (Early
327 Eocene) the average and seasonal amplitude in Mg/Ca is slightly lower around 4 mmol/mol. This
328 difference may be attributed to a palaeoenvironmental effect as these species lived during different
329 geological time intervals (early Eocene for *F. hemiglobosa* and the middle Eocene for *O. (T.) stric-*
330 *tiplicata*). However, it is more likely due to a species-specific effect on the magnesium incorporation
331 into the calcitic shell as clearly indicated below in our analyses comparing temperatures derived
332 from these results.

333 *5.3. Validity of Mg/Ca -temperature calibrations depending on species*

334 Mg/Ca-temperature calibrations have been successfully developed for different bivalve species
335 (e.g. fan mussel, mussel, scallop, and oyster; Table 1, Klein et al., 1996; Vander Putten et al.,
336 2000; Freitas et al., 2005, 2006, 2009, 2012; Wanamaker et al., 2008; Surge and Lohmann, 2008;
337 Mouchi et al., 2013). Given that these calibrations vary strongly between bivalves according on
338 the shell species (Figure 10), we will therefore only focus on calibrations established on modern
339 oyster species. For modern oysters, calibrations have been obtained by Surge and Lohmann (2008)
340 for the estuaries species *Crassostrea virginica* and by Mouchi et al. (2013) for the marine species
341 *Crassostrea gigas*. To apply these existing calibrations to the extinct fossil species, including those
342 analysed in this study, it is necessary to account for potential inter-species differences. To do
343 so, temperatures obtained using various existing oyster calibrations are compared to temperatures
344 estimated from measured $\delta^{18}O$. The carbonaceous shells of most bivalves are precipitated in isotopic
345 equilibrium with the seawater (e.g. Kirby et al., 1998) so that the oxygen isotopic composition of

different species can be directly compared. Thereby, relationships between seawater temperature, calcite $\delta^{18}O_c$, and seawater $\delta^{18}O_{sw}$ are commonly applied to estimate temperatures using fossil bivalve shells (e.g. Ivany et al., 2000; Gillikin et al., 2005). Here we apply calibration established by Anderson and Arthur (1983) between seawater temperature T (°C), bivalve calcite $\delta^{18}O_c$ (‰, VPDB), and seawater $\delta^{18}O_{sw}$ (‰, SMOW):

$$T = 16 - 4.14 \times (\delta^{18}O_c - \delta^{18}O_{sw}) + 0.13 \times (\delta^{18}O_c - \delta^{18}O_{sw})^2 \quad (1)$$

To estimate $\delta^{18}O_{sw}$ we used a range between the commonly accepted -1‰ value for global ice-free Eocene seawater (e.g. Ivany et al., 2000) and the more realistic value of 0.65‰ provided recently by numerical modelling near our study area at an Eocene position of 37.5°N, 71.25°E corresponding to the eastern Proto-Paratethys (Tindall et al., 2010). Resulting calculated seawater temperatures vary from approximately 22 to 41°C for average temperatures, ∼25 to 46°C for summer temperatures and ∼20 to 37°C for winter temperatures (Figure° 11).

Applying the Mg/Ca-temperature calibration for the extant oyster *C. virginica* (Surge and Lohmann, 2008) to our fossil oysters results in temperatures that are considerably lower than those based on $\delta^{18}O$ assuming a $\delta^{18}O_{sw}$ of 0.65‰ or even -1‰ (Figure 10). The application of this Mg/Ca-temperature calibration is therefore not suitable for any of the oyster species considered here, as was shown before on *S. buhsii* (Bougeois et al., 2014). In contrast, $\delta^{18}O$-derived temperatures compare better with those based for the Mg/Ca calibration of the marine oyster species *C. gigas* (Mouchi et al., 2013, Figure 10). Previous studies on calcifiers noticed that because seawater Mg/Ca was 50% of modern in the Palaeogene (3 mmol/mol compare to 5 mmol/mol in average), this could be a significant source of uncertainty which may have led to Palaeogene species being characterised by lower Mg/Ca ratios (Evans and Müller, 2012). However, the calibration done by (Mouchi et al., 2013) was established in Arcachon Basin were the seawater Mg/Ca is more or less 5 mmol/mol which is close to the modern seawater Mg/Ca ratio. Furthermore even for modern time, seawater Mg/Ca is highly variable (1) between open and coastal environment and (2) at an infra annual scale especially in coastal or near shore environment. According Lorens and Bender (1980) the relationship between Mg in the environment, in the biological fluids and in the calcitic part the carbonaceous shell is not clear (compare to Sr). Even if Mouchi et al. (2013) thermodependant equation do not include seawater Mg/Ca, Surge and Lohmann (2008) showed that a large variation of seawater Mg/Ca from 1 to 5 mmol/mol (due to the proximity of Mississipi delta) do not have a

significant influence on the oyster shell Mg/Ca. This encourage the sue of such calibrations, even in Palaeocene and Eocene times.

However, the validity of the calibration of Mouchi et al. (2013) varies between analysed species.

- Mg/Ca values from *O. bellovacina*, *F. hemiglobosa*, *P. asiatica* and *F. bashibulakeensis* appear to result in unrealistic temperatures using the calibration of Mouchi et al. (2013). Summer temperatures from specimens MS13-O23 (*F. hemiglobosa*) and KZ12-O12.2 (*O. bellovacina*) are unrealistically high (>50-60°C). Comparatively, the Mg/Ca- based temperatures for specimens KA12-O02.2 (*O. bellovacina*), MS12-O06.5 (*F. bashibulakeensis*), AB11-O01.1 (*P. asiatica*), AT12-O07B and TK11-O04 (both *F. hemiglobosa*) are unrealistically low (down to 10°C) compared to the δ^{18}O-based temperatures (32 to 40°C in average with a constant $\delta^{18}O_{sw}$ = 0.65‰, Figure 11b). An overestimation of $\delta^{18}O_{sw}$ of around -4‰ would be required to match the temperatures deduced from both proxies, which is very unlikely in an open marine environment. Furthermore, given the overall warm conditions for the Palaeocene-Eocene and particularly for the Central Asian sample location, temperatures as low as 10°C are not realistic (Lan, 1997; Sun and Wang, 2005; Guo et al., 2008; Tindall et al., 2010; Quan et al., 2012). We conclude that the Mg/Ca-temperature calibration of Mouchi et al. (2013) does not apply to shells of *O. bellovacina*, *F. hemiglobosa*, *P. asiatica* and *F. bashibulakeensis*. This suggests that incorporation of Mg differs significantly between species, even within the Ostreidae superfamily. Furthermore, specimens of the species *P. asiatica* analysed here were living in a marine environment under the influence of continental runoff (mangrove area, restricted marine waters, Figure 2). This may suggest also a potential additional impact from the environment on the magnesium incorporation for this species.

- *S. buhsii* and *O. (T.) strictiplicata*, in contrast, appear to yield reliable temperatures using the calibration of Mouchi et al. (2013) that are within the same range as those estimated using δ^{18}O (around 25 and 30°C in average with a $\delta^{18}O_{sw}$ = 0.65‰, Figure 11b). Considering that these species also provide the most reliable Mg/Ca records discussed above (Figure 6), we conclude that these species are particularly suitable for estimating palaeotemperatures.

Although average Mg/Ca-derived temperatures are comparable to those based on δ^{18}O, the seasonal amplitudes in temperature are significantly higher for Mg/Ca compared to δ^{18}O (Figure

11; also discussed in Bougeois et al., 2014) this likely relates to seasonal fluctuations in the $\delta^{18}O$ of seawater as expected in coastal marine living environments of the studied oysters according to the interpreted depositional palaeoenvironments. Indeed sedimentological (Manceau et al., 2014) and palynological (Sun and Wang, 2005; Guo et al., 2008; Quan et al., 2012) data indicate coeval arid to semi-arid conditions within evaporitic precipitation in playa and sabkha environments. These conditions are prone to seasonal fluctuations of salinity in subtidal environment which in turns regulate the $\delta^{18}O_{sw}$. Furthermore, the Mg-estimated temperatures are consistent with SST derived from numerical modelling for this area in the Eocene (Tindall et al., 2010) as well as SST in modern analogous environments previously studied with shell sclerochronology in the Upper Gulf of California (Goodwin et al., 2001) or the San Francisco Bay (Goodwin et al., 2012). Together, these observations suggest that the modern Mg/Ca-temperature calibration for *C. gigas* (Mouchi et al., 2013) can be applied to extinct fossil species of *O. (T.) strictiplicata* and *S. buhsii*. In general, this indicates that, after careful inspection of the diagenesis effect and independent characterization of the depositional environments, Mg-temperature calibrations based on modern specimens can be used to reconstruct past temperatures and seasonal patterns therein from fossil oyster shells.

6. Further development and conclusions

By comparing Mg/Ca to $\delta^{18}O$ high-resolution profiles from various fossil species in different depositional environments we devised a protocol to identify fossil species yielding reliable temperatures when using Mg/Ca-temperature calibrations derived from existing studies on modern oyster species.

The palaeobiogeographic distributional patterns of the reliable oyster species identified here (*S. buhsii* and *O. (T.) strictiplicata*) show an extraordinarily wide dispersal beyond the Tarim Basin into the regional Turkestan stage of Central Asia (Vyalov, 1937), in Northwest Afghanistan (Berizzi, 1970) and in northern Iran (Grewingk, 1853). Occurrences of Palaeogene oysters have also been reported in the Transylvanian Basin (Rusu et al., 2004) and as far west as the Paris Basin (for *O. bellovacina* Lan and Wei, 1995). This broad distribution makes these species an ideal choice to track palaeo-seasonality in a large area during the particular Palaeogene period, when global climate changed from greenhouse to icehouse conditions.

Combining Mg-estimated temperature with $\delta^{18}O$ allows reconstructions of seasonal variabil-

ity in $\delta^{18}O_{sw}$ ultimately reflecting changes in salinity (see equation 1 and supplementary data for these calculations, Bougeois et al., 2014). Seasonally-resolved salinity can be used for palaeoclimate interpretation of the basin hydrological cycle (evaporation and precipitation) at intra-annual resolution thereby significantly improving the comprehension of the environment compared to previous palaeontological studies as exemplified in our study area (Sun and Wang, 2005; Guo et al., 2008; Quan et al., 2012). Furthermore, by comparing Mg/Ca and $\delta^{18}O$ from multiple species from the same stratigraphic level, one could in principle statistically deconvolve impact of differences in sea water Mg/Ca or establish freshwater to seawater mixing lines from $\delta^{18}O$.

In principle, the protocol developed here is applicable to oyster (or even more largely bivalve) fossil species if they are found to yield reliable temperatures using the few existing temperature-calibrated modern species. The necessity to perform additional calibration studies on modern oyster species to improve calibrations for Mg/Ca and temperature for various Ostreidae species follows is underscored by our inconsistent results with *F. hemiglobosa* or *F. bashibulakeensis* species from which no reliable Mg-temperature could be extracted. Further calibration work may also help identify possible specific vital effect on Mg incorporation into the shell (already observed on modern species within a same genus such as *Mytilus* sp. or *Crassostrea* sp., Table 1), as well as the environmental impact (observed on same species *Pecten maximus* in different environment such as estuarine (Vander Putten et al., 2000), culturing (Freitas et al., 2008) or brackish (Wanamaker et al., 2008)). Furthermore, these studies will certainly benefit from the calibration of other trace elements and isotopes such as Ba and $\delta^{13}C$ recently used as indicators of primary productivity (Goodwin et al., 2012).

Improving the knowledge on biomineralisation of Ostreidae shells is a prime target to develop a reliable and powerful environmental proxies. Indeed, the widespread occurrence of Ostreidae in the fossil records in terms of age (from Triassic until Quaternary) and of geolocalisation (from low to high latitudes, from brackish to fully marine environments) make Ostreidae the most promising group to infer palaeenvironments at intra-annual resolution.

7. Acknowledgements

This project was partly funded by the Netherlands Organization for Scientific Research (NWO), the A. v. Humboldt foundation and the Marie Curie Career Integration Grant HIRESDAT. We

are grateful to the CaiYuanpei programme of the French ministry of foreign affairs for collaborative support in field excursion. We would like to thank Roderic Bosboom, Gloria Heilbronn, Bruno Paulet and Jean-Noël Proust for their contribution in the field. We are grateful to Helen de Waard, Arnold Van Dijk for their help during experiments with LA-ICP-MS and stable isotopes analyses in Utrecht University. We are grateful to Nathalie Labourdette and Catherine Pierre for their help during experiments with stable isotopes analyses and Micromill access in Pierre et Marie Curie University.

References

Anderson, T., Arthur, M., 1983. Stable isotopes of oxygen and carbon and their application to sedimentologic and paleoenvironmental problems. Stable isotopes in sedimentary geology 10, 1–151.

Berizzi, Quarto di Palo, A., 1970. Paleogene pelecypods from Kataghan and Badakhshan (North-East Afganistan). Fossils of North-East Afganistan: Italian Expeditions to the Karakorum (K2), and Hindu Kush, IV/2:. Brill. Desio, A. , 161–240.

Bosboom, R., Dupont-Nivet, G., Grothe, A., Brinkhuis, H., Villa, G., Mandic, O., Stoica, M., Huang, W., Yang, W., Guo, Z., Krijgsman, W., 2014a. Linking Tarim Basin sea retreat (west China) and Asian aridification in the late Eocene. Basin Research .

Bosboom, R., Dupont-Nivet, G., Grothe, A., Brinkhuis, H., Villa, G., Mandic, O., Stoica, M., Kouwenhoven, T., Huang, W., Yang, W., et al., 2014b. Timing, cause and impact of the late Eocene stepwise sea retreat from the Tarim Basin (west China). Palaeogeography, Palaeoclimatology, Palaeoecology .

Bosboom, R., Dupont-Nivet, G., Mandic, O., Proust, J., Ormukov, C., 2014c. Late Eocene paleogeography of the Proto-Paratethys Sea in Central Asia (NW China, S Kyrgyzstan and SW Tajikistan). Geological Society of London Special Publications .

Bougeois, L., de Rafélis, M., Reichart, G.J., de Nooijer, L.J., Nicollin, F., Dupont-Nivet, G., 2014. A high resolution study of trace elements and stable isotopes in oyster shells to estimate Central Asian Middle Eocene seasonality. Chemical Geology 363, 200–212.

Burtman, V., 2000. Cenozoic crustal shortening between the Pamir and Tien Shan and a reconstruction of the Pamir–Tien Shan transition zone for the Cretaceous and Palaeogene. Tectonophysics 319, 69–92.

Carter, J.G., Altaba, C.R., Anderson, L., Araujo, R., Biakov, A.S., Bogan, A.E., Campbell, D.C., Campbell, M., Chen, J.h., Cope, J.C., et al., 2011. A synoptical classification of the bivalvia (mollusca). University of Kansas Paleontological Contributions, .

De Rafélis, M., Renard, M., Emmanuel, L., Durlet, C., 2000. Contribution of cathodoluminescence to the knowledge of manganese speciation into pelagic limestones. Determination of the control of sea-level variations on third-order sequences during the Upper Jurassic. Comptes Rendus de l'Académie des Sciences Series IIA Earth and Planetary Science 330, 391–398.

Dercourt, J., Ricou, L.E., Vrielynck, B., 1993. Atlas Tethys, Paleoenvironmental Maps: Explanatory Notes. Gauthier-Villars.

Dodd, J., 1965. Environmental control of strontium and magnesium in *Mytilus*. Geochimica et Cosmochimica Acta 29, 385–398.

El Ali, A., Barbin, V., Calas, G., Cervelle, B., Ramseyer, K., Bouroulec, J., 1993. Mn^{2+}-activated luminescence in dolomite, calcite and magnesite: quantitative determination of manganese and site distribution by EPR and CL spectroscopy. Chemical Geology 104, 189–202.

Elderfield, H., Ganssen, G., 2000. Past temperature and $\delta^{18}O$ of surface ocean waters inferred from foraminiferal Mg/Ca ratios. Nature 405, 442–445.

Eldrett, J.S., Harding, I.C., Wilson, P.A., Butler, E., Roberts, A.P., 2007. Continental ice in greenland during the eocene and oligocene. Nature 446, 176–179.

Evans, D., Müller, W., 2012. Deep time foraminifera Mg/Ca paleothermometry: Nonlinear correction for secular change in seawater Mg/Ca. Paleoceanography 27.

Evans, D., Müller, W., Oron, S., Renema, W., 2013. Eocene seasonality and seawater alkaline earth reconstruction using shallow-dwelling large benthic foraminifera. Earth and Planetary Science Letters 381, 104–115.

Felis, T., Lohmann, G., Kuhnert, H., Lorenz, S.J., Scholz, D., Pätzold, J., Al-Rousan, S.A., Al-Moghrabi, S.M., 2004. Increased seasonality in middle east temperatures during the last interglacial period. Nature 429, 164–168.

Freitas, P., Clarke, L., Kennedy, H., Richardson, C., 2008. Inter-and intra-specimen variability masks reliable temperature control on shell Mg/Ca ratios in laboratory and field cultured *Mytilus edulis* and *Pecten maximus* (bivalvia). Biogeosciences Discussions 5.

Freitas, P., Clarke, L., Kennedy, H., Richardson, C., 2009. Ion microprobe assessment of the heterogeneity of Mg/Ca, Sr/Ca and Mn/Ca ratios in *Pecten maximus* and *Mytilus edulis* (bivalvia) shell calcite precipitated at constant temperature. Biogeosciences Discussions 6.

Freitas, P., Clarke, L., Kennedy, H., Richardson, C., Abrantes, F., 2005. Mg/Ca, Sr/Ca, and stable-isotope (δ^{18}O and δ^{13}C) ratio profiles from the fan mussel *Pinna nobilis*: Seasonal records and temperature relationships. Geochemistry Geophysics Geosystems 6, Q04D14.

Freitas, P., Clarke, L., Kennedy, H., Richardson, C., Abrantes, F., 2006. Environmental and biological controls on elemental (Mg/Ca, Sr/Ca and Mn/Ca) ratios in shells of the king scallop *Pecten maximus*. Geochimica et Cosmochimica Acta 70, 5119–5133.

Freitas, P.S., Clarke, L.J., Kennedy, H., Richardson, C.A., 2012. The potential of combined Mg/Ca and δ^{18}O measurements within the shell of the bivalve *Pecten maximus* to estimate seawater δ^{18}O composition. Chemical Geology 291, 286–293.

Gillikin, D., De Ridder, F., Ulens, H., Elskens, M., Keppens, E., Baeyens, W., Dehairs, F., 2005. Assessing the reproducibility and reliability of estuarine bivalve shells (*Saxidomus giganteus*) for sea surface temperature reconstruction: Implications for paleoclimate studies. Palaeogeography, Palaeoclimatology, Palaeoecology 228, 70–85.

Goodwin, D., Gillikin, D., Roopnarine, P., 2012. Preliminary evaluation of potential stable isotope and trace element productivity proxies in the oyster *Crassostrea gigas*. Palaeogeography, Palaeoclimatology, Palaeoecology .

Goodwin, D.H., Flessa, K.W., Schöne, B.R., Dettman, D.L., 2001. Cross-calibration of daily growth increments, stable isotope variation, and temperature in the Gulf of California bivalve mollusk *Chione cortezi*: implications for paleoenvironmental analysis. Palaios 16, 387–398.

Grewingk, 1853. Die geognostischen und geographischen Verhältnisse des nordlichen Persiens. Verhandlungen der Russisch-Kaiserlichen mineralogischen Gesellschaft zu St. Petersburg , 97–245.

Guo, Z., Sun, B., Zhang, Z., Peng, S., Xiao, G., Ge, J., Hao, Q., Qiao, Y., Liang, M., Liu, J., et al., 2008. A major reorganization of asian climate by the early miocene. Climate of the Past 4.

Habermann, D., 2002. Quantitative cathodoluminescence (CL) spectroscopy of minerals: possibilities and limitations. Mineralogy and Petrology 76, 247–259.

Hathorne, E.C., James, R.H., Savage, P., Alard, O., 2008. Physical and chemical characteristics of particles produced by laser ablation of biogenic calcium carbonate. Journal of Analytical Atomic Spectrometry 23, 240–243.

Hudson, J., Shinn, E., Halley, R., Lidz, B., 1976. Sclerochronology: a tool for interpreting past environments. Geology 4, 361–364.

Ivany, L., Patterson, W., Lohmann, K., 2000. Cooler winters as a possible cause of mass extinctions at the Eocene/Oligocene boundary. Nature 407, 887–890.

Jochum, K.P., Weis, U., Stoll, B., Kuzmin, D., Yang, Q., Raczek, I., Jacob, D.E., Stracke, A., Birbaum, K., Frick, D.A., et al., 2011. Determination of reference values for NIST SRM 610–617 glasses following ISO guidelines. Geostandards and Geoanalytical Research 35, 397–429.

Killingley, J.S., Berger, W.H., 1979. Stable isotopes in a mollusk shell: detection of upwelling events. Science 205, 186–188.

Kirby, M.X., 2001. Differences in growth rate and environment between tertiary and quaternary *Crassostrea* oysters. Journal Information 27.

Kirby, M.X., Soniat, T.M., Spero, H.J., 1998. Stable isotope sclerochronology of Pleistocene and Recent oyster shells (Crassostrea virginica). Palaios 13, 560–569.

Klein, R., Lohmann, K., Thayer, C., 1996. Bivalve skeletons record sea-surface temperature and $\delta^{18}O$ via Mg/Ca and $^{18}O/^{16}O$ ratios. Geology 24, 415–418.

Lan, X., 1997. Paleogene bivalve communities in the Western Tarim Basin and their paleoenvironmental implications. Paleoworld , 137–157.

569 Lan, X., Wei, J., 1995. Late Cretaceous–early Tertiary marine bivalve fauna from the western Tarim
570 Basin .

571 Langlet, D., Alunno-Bruscia, M., de Rafélis, M., Renard, M., Roux, M., Schein, E., Buestel, D.,
572 et al., 2006. Experimental and natural manganese-induced cathodoluminescence in the shell of
573 the Japanese oyster *Crassostrea gigas* (Thunberg, 1793) from Thau Lagoon (Hérault, France):
574 ecological and environmental implications. Marine Ecology-Progress Serie 317, 143–156.

575 Lartaud, F., Emmanuel, L., De Rafelis, M., Pouvreau, S., Renard, M., 2010a. Influence of food sup-
576 ply on the δ^{13}c signature of mollusc shells: implications for palaeoenvironmental reconstitutions.
577 Geo-Marine Letters 30, 23–34.

578 Lartaud, F., de Rafélis, M., Ropert, M., Emmanuel, L., Geairon, P., Renard, M., 2010b. Mn
579 labelling of living oysters: Artificial and natural cathodoluminescence analyses as a tool for age
580 and growth rate determination of *C. gigas* (Thunberg, 1793) shells. Aquaculture 300, 206–217.

581 Lear, C.H., Elderfield, H., Wilson, P., 2000. Cenozoic deep-sea temperatures and global ice volumes
582 from mg/ca in benthic foraminiferal calcite. Science 287, 269–272.

583 Licht, A., van Cappelle, M., Abels, H.A., Ladant, J.B., Trabucho-Alexandre, J., France-Lanord, C.,
584 Donnadieu, Y., Vandenberghe, J., Rigaudier, T., Lécuyer, C., Terry Jr, D., Adriaens, R., Boura,
585 A., Guo, Z., Soe, A.N., Quade, Z., Dupont-Nivet, G., Jaeger, J.J., 2014. Asian monsoons in a
586 late Eocene greenhouse world. Nature Geosciences .

587 Lorens, R.B., Bender, M.L., 1980. The impact of solution chemistry on *Mytilus edulis* calcite and
588 aragonite. Geochimica et Cosmochimica Acta 44, 1265–1278.

589 Lough, J., 2010. Climate records from corals. Wiley Interdisciplinary Reviews: Climate Change 1,
590 318–331.

591 Manceau, C., Bougeois, L., Proust, J.N., Dupont-Nivet, G., 2014. Evolution des environnements de
592 dépôts dans le bassin du Tarim (Chine) au cours du retrait Paléogène de la Proto-Paratethys, in:
593 24ème Réunion des sciences de la Terre 2014, pp. 67–68.

594 Mouchi, V., de Rafélis, M., Lartaud, F., Fialin, M., Verrecchia, E., 2013. Chemical labelling of

oyster shells used for time-calibrated high-resolution Mg/Ca ratios: A tool for estimation of past seasonal temperature variations. Palaeogeography, Palaeoclimatology, Palaeoecology 373, 66–74.

Nürnberg, D., Bijma, J., Hemleben, C., 1996. Assessing the reliability of magnesium in foraminiferal calcite as a proxy for water mass temperatures. Geochimica et Cosmochimica Acta 60, 803–814.

Quan, C., Liu, Y., Utescher, T., 2012. Eocene monsoon prevalence over china: A paleobotanical perspective. Palaeogeography, Palaeoclimatology, Palaeoecology .

Richardson, C., 2001. Molluscs as archives of environmental change. Oceanogr. Mar. Biol. Annu. Rev 39, 103–164.

Richardson, C., Collis, S., Ekaratne, K., Dare, P., Key, D., 1993. The age determination and growth rate of the european flat oyster, *Ostrea edulis*, in british waters determined from acetate peels of umbo growth lines. ICES Journal of Marine Science: Journal du Conseil 50, 493–500.

Rosenberg, G., Hughes, W., 1991. A metabolic model for the determination of shell composition in the bivalve mollusc *Mytilus edulis*. Lethaia 24, 83–96.

Rusu, A., Brotea, D., Melinte, M.C., 2004. Biostratigraphy of the Bartonian deposits from Gilău area (NW Transylvania, Romania). Acta Palaeontologica Romaniae 4, 441–454.

Schöne, B.R., Zhang, Z., Jacob, D., Gillikin, D.P., Tütken, T., Garbe-Schönberg, D., Mcconnaughey, T., Soldati, A., 2010. Effect of organic matrices on the determination of the trace element chemistry (mg, sr, mg/ca, sr/ca) of aragonitic bivalve shells (arctica islandica)—comparison of icp-oes and la-icp-ms data. Geochemical Journal 44, 23.

Stenzel, H.B., 1971. Oysters. Treatise on invertebrate paleontology 3, 953–1184.

Sun, X., Wang, P., 2005. How old is the Asian monsoon system? Palaeobotanical records from China. Palaeogeography, Palaeoclimatology, Palaeoecology 222, 181–222.

Surge, D., Lohmann, K., 2008. Evaluating Mg/Ca ratios as a temperature proxy in the estuarine oyster, *Crassostrea virginica*. Journal of Geophysical Research 113, G02001.

Surge, D., Lohmann, K., Dettman, D., 2001. Controls on isotopic chemistry of the American oyster, *Crassostrea virginica*: implications for growth patterns. Palaeogeography, Palaeoclimatology, Palaeoecology 172, 283–296.

Tindall, J., Flecker, R., Valdes, P., Schmidt, D., Markwick, P., Harris, J., 2010. Modelling the oxygen isotope distribution of ancient seawater using a coupled ocean-atmosphere GCM: implications for reconstructing early Eocene climate. Earth and Planetary Science Letters 292, 265–273.

Vander Putten, E., Dehairs, F., Keppens, E., Baeyens, W., 2000. High resolution distribution of trace elements in the calcite shell layer of modern *Mytilus edulis*: environmental and biological controls. Geochimica et Cosmochimica Acta 64, 997–1011.

Vyalov, O., 1937. Sur la Clasification des Ostréidés et leur Valeur stratigraphique. XIIe Congrès Internationnal de Zoologie Session VIII, 1627–1638.

Wanamaker, A.D., Kreutz, K.J., Wilson, T., Borns Jr, H.W., Introne, D.S., Feindel, S., 2008. Experimentally determined mg/ca and sr/ca ratios in juvenile bivalve calcite for *Mytilus edulis*: implications for paleotemperature reconstructions. Geo-Marine Letters 28, 359–368.

Wefer, G., Berger, W.H., 1991. Isotope paleontology: growth and composition of extant calcareous species. Marine geology 100, 207–248.

Tables and Figures

Table 1: Comparison of Mg/Ca–seawater temperature relationships for calcitic bivalves.

Table 2: Summary of experiments performed on the 41 oyster slabs. The three last columns indicate the reliability of Mg/Ca transects based on the two main characteristics : Intra-shell variability ans Signal cyclicity ("+", "=" and "−" correspond respectively to suitable, partly suitable and unsuitable signal). The reliability of the Mg/Ca result for each oyster is expressed by: S = suitable, PS = partly suitable, US = unsuitable.

Figure 1: **a.** Location of sampling area in Kyrgyzstan (yellow), Tajikistan (blue) and China (orange). **b.** Middle Eocene Palaeographical map showing Central Asia invaded by the Proto-Paratethys sea (map from Licht et al., 2014). **c.** Position of analysed species on schematic illustration of the third to fifth marine incursions into the Tarim basin (Bosboom et al., 2014b). **d.** Examples of analysed fossil oyster left valves with well-developed ligamental area. **(i.)** *F. hemiglobosa*, **(ii.)** *O. (T.) strictiplicata*, **(iii.)** *S. buhsii*, **(iv.)** *P. asiatica*, **(v).** *F. bashibulakeensis*. The first part of the specimen's name indicates the provenance with the code of the stratigraphic sections (see section codes below), and the year of sampling. The complete list of oysters from Central Asia analysed in this study is available in supplementary data. Code for stratigraphic sections - MS: Mine-Bashibulake (39° 51'N, 74° 32'E), KA: Kansu (39° 45'N, 74° 58'E), KZ: Kezi (38° 26'N, 76° 24'E), AT: Aertashi (37° 58'N, 76° 33'E), YK: Yarkand (37.7° N, 76.6° E), KY: Keyliand (37° 27'N, 77° 86'E), AB: Ala Buka (41.4° N, 71.4° E), TK: Tash Kumyr (41.3° N, 72.2° E), AL: Alai Valley (39.6° N, 72.4° E), UT: Uch Tobo (39.9° N, 73.4° E), DS: Kuhdara-Dushanbe (38.7° N, 68.9° E).

Figure 2: **a.** Environment of the studied species: age, formation, depositional environment and associated fauna. **b.** Living position of species through the carbonate platform.

Figure 3: Radial sections (top) of oyster ligamental areas showing light and dark alternations, each couplet corresponding to one living growth years. Cathodoluminescence assemblages (bottom) for these specimens show alternation of areas with high and low luminescence corresponding to light and dark bands observed in natural light. Transects followed by laser ablation for trace element analyses are indicated in blue and green. Main paths followed by the Micromill for stable isotopes analyses are indicated in black. Black arrows indicate growth directions. (a.) *O. bellovacina*, (b.) *F. hemiglobosa* , (c.) *S. buhsii* and (d.) *F. bashibulakeensis*. Supplementary data provides the radial sections and CL images of complete collection. **e.** Geochemical data for the specimen KZ12-O03 (*S. buhsii*): Cathodoluminescence grey scale (light red: raw data, dark red: moving average) results, Mg/Ca ratio for two parallel transects yielding similar results (light blue or green: raw data, dark blue or green: moving average), Oxygen stable isotopes from the selected area. Grey areas correspond to light and dark layers as revealed by CL.

Figure 4: Geochemical data for the specimen KZ12-O03 (*S. buhsii*): Cathodoluminescence grey scale (light red: raw data, dark red: moving average) results, Mg/Ca ratio for two parallel transects yielding similar results (light blue or green: raw data, dark blue or green: moving average), Oxygen stable isotopes from the selected area. Grey areas correspond to light and dark layers as revealed by CL.

Figure 5: Incremental stable oxygen ratio records ($\delta^{18}O$) in oyster shells. Horizontal axis indicates distance in millimetres starting from the first drilled micro-sample. Grey areas correspond to visible dark bands on the shells, white areas correspond to the light bands revealed by CL analyses.

Figure 6: Suitable Mg/Ca result across the oyster shell ligamental area showing both well-expressed cyclicity and low intra-shell variability between parallel transects (Figure 3). Analyses were performed following the growth direction with 0 mm corresponding to the most juvenile part analysed. See Figure 8 for explanatory legend of used symbols and patterns.

Figure 7: Partly suitable Mg/Ca results across the oyster shell ligamental area showing only parts with well-expressed cyclicity and low intra-shell variability between parallel transects (Figure 3). Analyses were performed following the growth direction with 0 mm corresponding to the most juvenile part analysed.

Figure 8: Unsuitable Mg/Ca results across the oyster shell ligamental area showing poorly-expressed cyclicity and high intra-shell variability between parallel transects (Figure 3) of oyster shells. Analyses were performed following the growth direction with 0 mm corresponding to the most juvenile part analysed. See Figure 8 for explanatory legend of used symbols and patterns.

Figure 9: **a.-d.** $\delta^{18}O$ results from bulk and incremental analyses per stratigraphic section. **e.-h.** Mg/Ca results from incremental analyses per stratigraphic section. When the seasonal pattern could not be defined, we represented only the average (full black square) and a black line between the highest and the lowest values. Red depicts suitable signal, blue partly suitable signal and grey unsuitable signal. When oysters are coming from the same bed, the estimated age is the same. However, to better see the difference between them, we juxtaposed results next to each other. Numbers correspond to the Reference N° in Table 2. **i.** $\delta^{13}C$ vs $\delta^{18}O$ for bulk and averaged incremental results. Two groups can be clearly distinguished between relatively high (full line) and low (dashed line) values of $\delta^{18}O$ and $\delta^{13}C$. **j.** Compiled Mg/Ca results from the complete collection with suitable and partly suitable criteria.

Figure 10: **a.** Infra-annual temperatures (0.2 mm moving average) for the specimen AT13-O20 estimated using various Mg/Ca calibrations established on different species of calcitic bivalves (1 to 10, cf Table 1), or using $\delta^{18}O$ calibration of Anderson and Arthur (1983) with a constant $\delta^{18}O_{sw}$ of 0.65‰ according to modelled values for the study area in the Eocene (Tindall et al., 2010) (11), or of -1‰ according to the value commonly used for the Eocene ice free world (12). **b.** Associated temperature range for each calibration.

Figure 11: **a.** Estimated temperature using Mg/Ca ratio with the calibration of Mouchi et al. (2013) (red line; in order to not overcrowd the graphs, only the moving average of Mg estimated temperature are shown) compared to estimated temperature using $\delta^{18}O$ with the calibration of Anderson and Arthur (1983) and with a constant $\delta^{18}O_{sw}$ of 0.65‰ (green plain circles) or -1‰ (orange empty circles). Grey areas correspond to dark bands on the shells. **b.** Comparison between range of temperatures deduced from Mg/Ca (Mouchi et al., 2013) and $\delta^{18}O$ (Anderson and Arthur, 1983) with a constant $\delta^{18}O_{sw}$ of 0.65‰.

Species	Environment	Temperature range	Mg/Ca =f(T)	Reference
Pinna nobilis	marine	10-22 °C	Mg/Ca = 17.16 (±1.95) * exp(0.022 (±0.004) * T)	Freitas et al., 2005 (1)
Pecten maximus	culturing	10-20 °C	Mg/Ca = 2.56 (±0.42) + 0.17 (±0.03) * T	Freitas et al., 2012 (2)
	marine	5-19°C	Mg/Ca = 4.92 (±2.16) + 0.50 (±0.16) * T	Freitas et al., 2006 (3)
	culturing	10-20 °C	Mg/Ca = 9.89 (±2.96) + 0.51 (±0.19) * T	Freitas et al., 2008 (4)
Mytilus trossolus	marine	6-23°C	Mg/Ca = 2.25 (±0.63) + 0.30 (±0.04) * T	Klein et al., 1996 (5)
Mytilus edulis	estuarine	5-20°C	Mg/Ca = -0.63 (±0.29) + 0.70 (±0.02) * T	Vander Putten., 2000 (6)
	culturing	10-20 °C	Mg/Ca = 1.50 (±0.57) + 0.27 (±0.04) * T	Freitas et al., 2008 (7)
	brakish water	7-19°C	Mg/Ca = 5.44 (±0.31) + 0.77 (±0.22) * T	Wanamaker et al., 2008 (8)
Crassostrea gigas	marine	5-25°C	Mg/Ca = -0.50 + 0.27 * T	Mouchi et al., 2013 (9)
Crassostrea virginica	estuarine	18-32°C	Mg/Ca = -0.23 + 0.72 * T	Surge et al., 2008 (10)

Bougeois et al., 2015
Table 1

Table 2

Section	Age	# Sample	Ref. N°	Species	CL	Bulk isotopes	Incremental isotopes	LA – ICP MS	Intra-shell variability	Cyclicity	Pattern
Kanzu	Thanetian	KA12-O02.1	1	*O. bellovacina*	✔	✔		✔	+	=	PS
	Thanetian	KA12-O02.2	2	*O. bellovacina*	✔	✔	✔	✔	+	=	PS
Mine	Ypresian	MS12-O15	3	*F. hemiglobosa*	✔	✔		✔	=	+	PS
	Ypresian	MS13-O23	4	*F. hemiglobosa*	✔	✔	✔	✔	−	−	US
	Early Lutetian	MS12-O05.2	5	*O. strictiplicata*	✔	✔	✔	✔	+	+	**S**
	Early Lutetian	MS10-O02.1	6	*O. strictiplicata*	✔	✔					
	Early Lutetian	MS13-O22	7	*O. strictiplicata*	✔	✔		✔	+	+	**S**
	Late Lutetian	MS12-O10.2	8	*S. buhsii*	✔	✔		✔	−	−	US
	Late Lutetian	MS10-O03	9	*S. buhsii*	✔	✔					
	Late Lutetian	MS13-O20	10	*S. buhsii*	✔	✔	✔	✔	+	=	PS
	Early Priabonian	MS12-O06.2	11	*F. bashibulakeensis*	✔	✔		✔	−	−	US
	Early Priabonian	MS12-O06.5	12	*F. bashibulakeensis*	✔	✔	✔	✔	=	+	PS
	Early Priabonian	MS10-O04	13	*F. bashibulakeensis*	✔	✔		✔	−	−	US
	Early Priabonian	MS13-O21	14	*F. bashibulakeensis*	✔	✔		✔	=	−	US
Aertashi	Ypresian	AT12-O07.A	15	*F. hemiglobosa*	✔			✔	+	=	PS
	Ypresian	AT12-O07.B	16	*F. hemiglobosa*	✔	✔	✔	✔	=	=	PS
	Ypresian	AT13-O21	17	*F. hemiglobosa*	✔	✔		✔	+	−	US
	Middle Lutetian	AT12-O09.2	18	*S. buhsii*	✔	✔		✔	+	+	**S**
	Middle Lutetian	AT12-O09.3	19	*S. buhsii*	✔	✔	✔	✔	+	+	**S**
	Middle Lutetian	AT13-O20	20	*O. strictiplicata*	✔	✔	✔	✔	+	+	**S**
	Late Lutetian	AT12-O15.1	21	*S. buhsii*	✔	✔		✔	−	−	US
	Late Lutetian	AT12-O015.2	22	*S. buhsii*	✔	✔	✔	✔	+	+	**S**
	Late Lutetian	AT13-O19	23	*S. buhsii*	✔	✔	✔	✔	+	+	**S**
	Late Lutetian	AT12-O18	24	*S. buhsii*	✔	✔		✔	=	+	PS
	Late Lutetian	AT11-O04	25	*S. buhsii*	✔	✔	✔	✔	+	+	**S**
Kezi	Thanetian	KZ12-O12.2	26	*O. bellovacina*	✔	✔	✔	✔	−	+	US
	Middle Lutetian	KZ12-O05.1	27	*S. buhsii*	✔	✔	✔	✔	−	+	US
	Late Lutetian	KZ12-O03	28	*S. buhsii*	✔	✔	✔	✔	+	+	**S**
	Late Lutetian	KZ07-O01	29	*S. buhsii*	✔	✔	✔	✔	=	+	PS
Keyliand	Late Lutetian	KY10-O01	30	*S. buhsii*	✔	✔	✔	✔	+	+	**S**
Yarkand	Ypresian	YK11-O01.1	31	*F. hemiglobosa*	✔	✔		✔	=	+	PS
Kuhdara	Ypresian	DS12-O01.2A	32	*F. hemiglobosa*	✔	✔		✔	−	−	US
	Ypresian	DS12-O01.2B	33	*F. hemiglobosa*	✔	✔		✔	=	−	US
	Ypresian	DS12-O01.3	34	*F. hemiglobosa*	✔	✔		✔	−	−	US
	Ypresian	DS12-O01.4	35	*F. hemiglobosa*	✔	✔		✔	−	−	US
	Ypresian	DS12-O01.5	36	*F. hemiglobosa*	✔	✔	✔	✔	−	=	US
Tash-Kumyr - Uch Tobo -Alai Valley - Ala Buka	Ypresian	TK11-O04	37	*F. hemiglobosa*		✔	✔	✔	=	=	PS
	Early Lutetian	AL11-O02.1	38	*O. strictiplicata*	✔	✔	✔	✔	+	+	**S**
	Early Lutetian	UT11-O01.1	39	*S. orientalis*	✔	✔		✔	−	−	US
	Early Lutetian	UT11-O02.1	40	*S. orientlis*	✔	✔		✔	+	+	**S**
	Late Lutetian	TK11-O03.2	41	*S. buhsii*	✔	✔		✔	=	+	PS
	Late Bartonian	AB11-O01.1	42	*P. asiatica*		✔	✔	✔	=	+	PS
	Late Bartonian	AB11-O01.2	43	*P. asiatica*		✔		✔	=	=	US

Figure 1

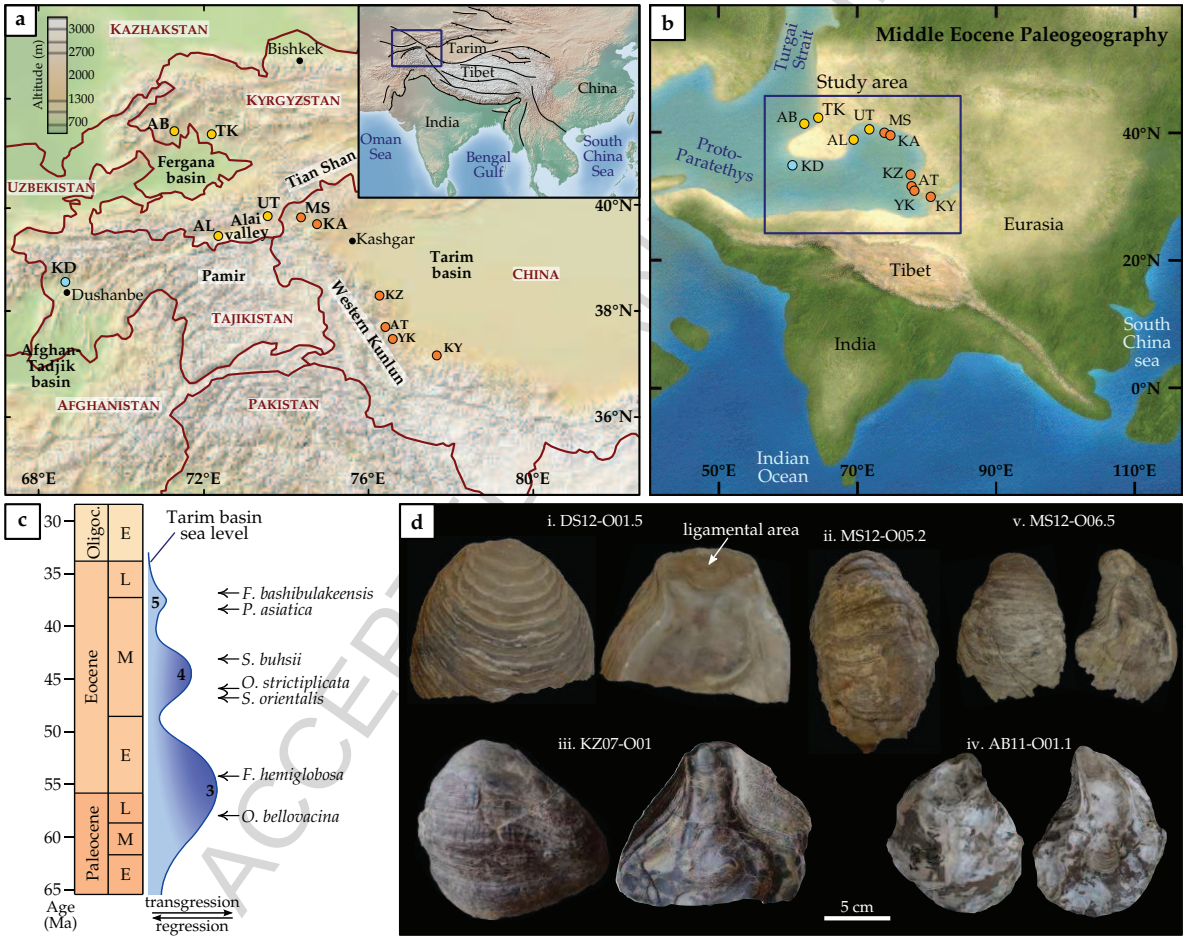

Bougeois et al., 2015
Figure 1

a

Species	Age	Formation	Environment	Sediment	Main associated fauna
Ostrea bellovacina (Lamarck, 1896)	Thanetian	Lower Qimugen	shoreface	oolithic bioclastic wackestone	*Pycnodonte nomada*, Bryozoa, Ostracodes, Algae, Urchin spines
Flemingostrea hemiglobosa (Romanovskiy, 1884)	Ypresian	Lower Qimugen	offshore or quiet bay	green marls	Foraminifera, Echinoids, Bryozoa, Fish scales
Sokolowia orientalis (Gekker, Osipova & Balskaya, 1962)	Early Lutetian	Kalatar	intertidal	bioclastic wackestone	*Ostrea afghanica*
Ostrea (T.) strictiplicata (Roulin and Delbos, 1855)	Early to Middle Lutetian	Kalatar	subtidal reef	bioclastic wackestone	*Ostrea (T.) cizancourt*i, Gastropods, Bryozoa, algae
Sokolowia buhsii (Grewingk, 1853)	Early to Middle Lutetian	Wulagen	offshore	green mudstones	Foraminifera, Echinoids, Briozoa, Serpulids, Sponge, *Chlamys* sp., *Kokanostrea kokanensis*
Platygena asiatica (Romanovskiy, 1879)	Late Bartonian	Bashibulake	mangrove	bioturbated sandy siltstones	*Cubisostrea plicata*, roots
Ferganea bashibulakeensis (Wei, 1984)	Early Priabonian	Bashibulake	subtidal or restricted marine	bluish marly siltstones	Lithophaga, Foraminifera, *Chlamys* sp.

b

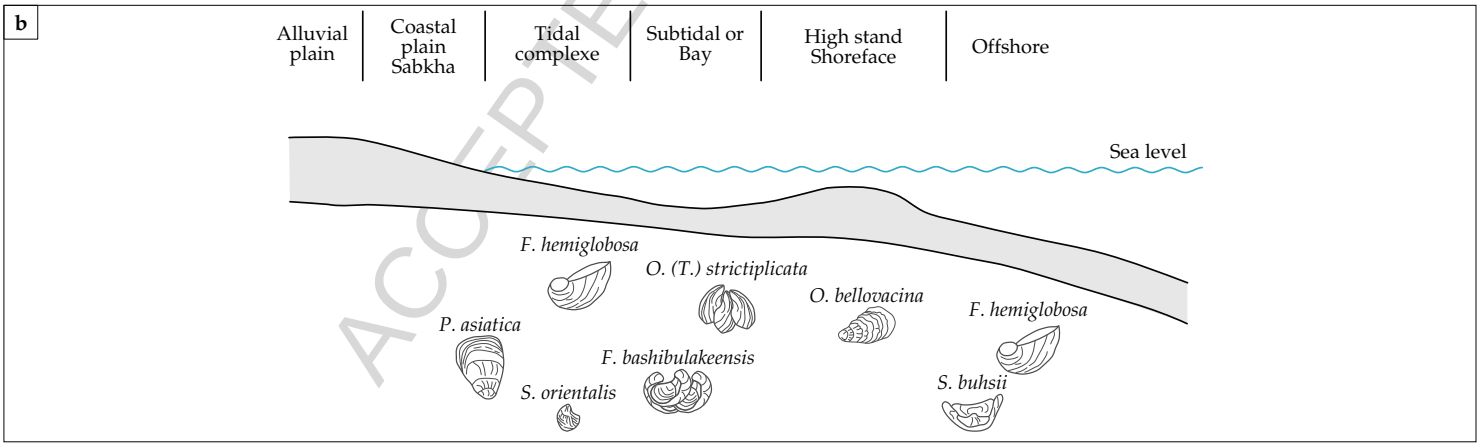

Bougeois et al., 2015
Figure 2

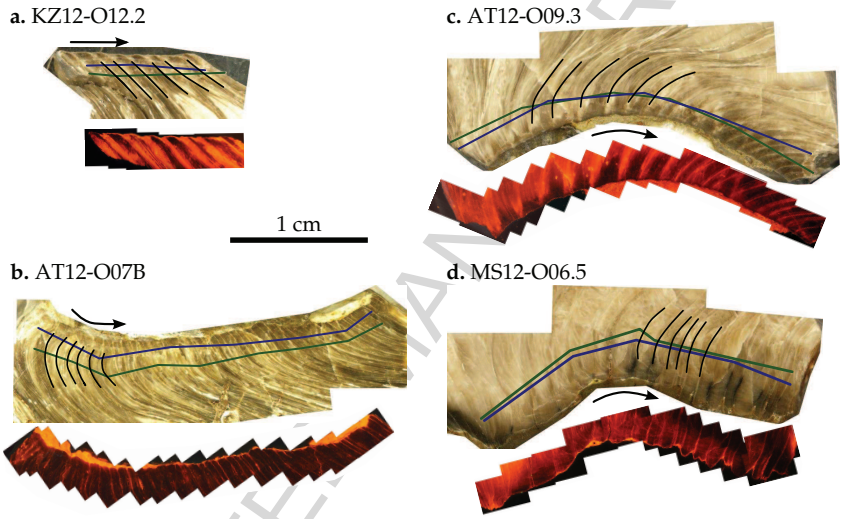

Bougeois et al., 2015
Figure 3

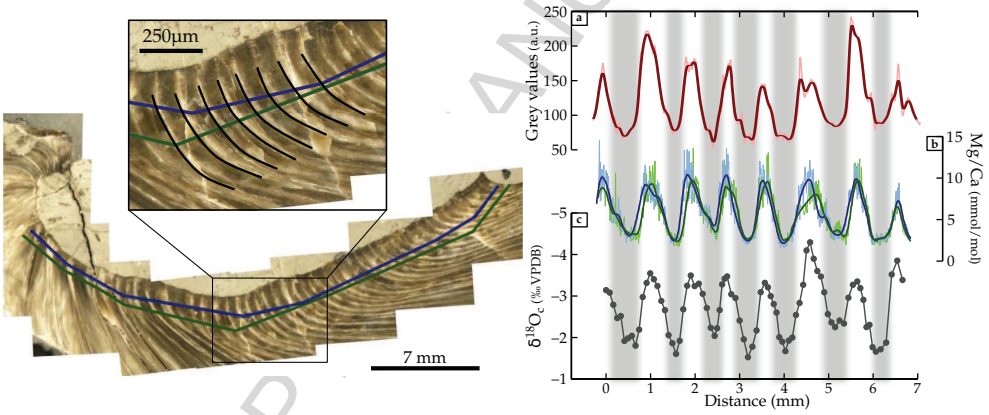

Bougeois et al., 2015
Figure 4

Figure 5

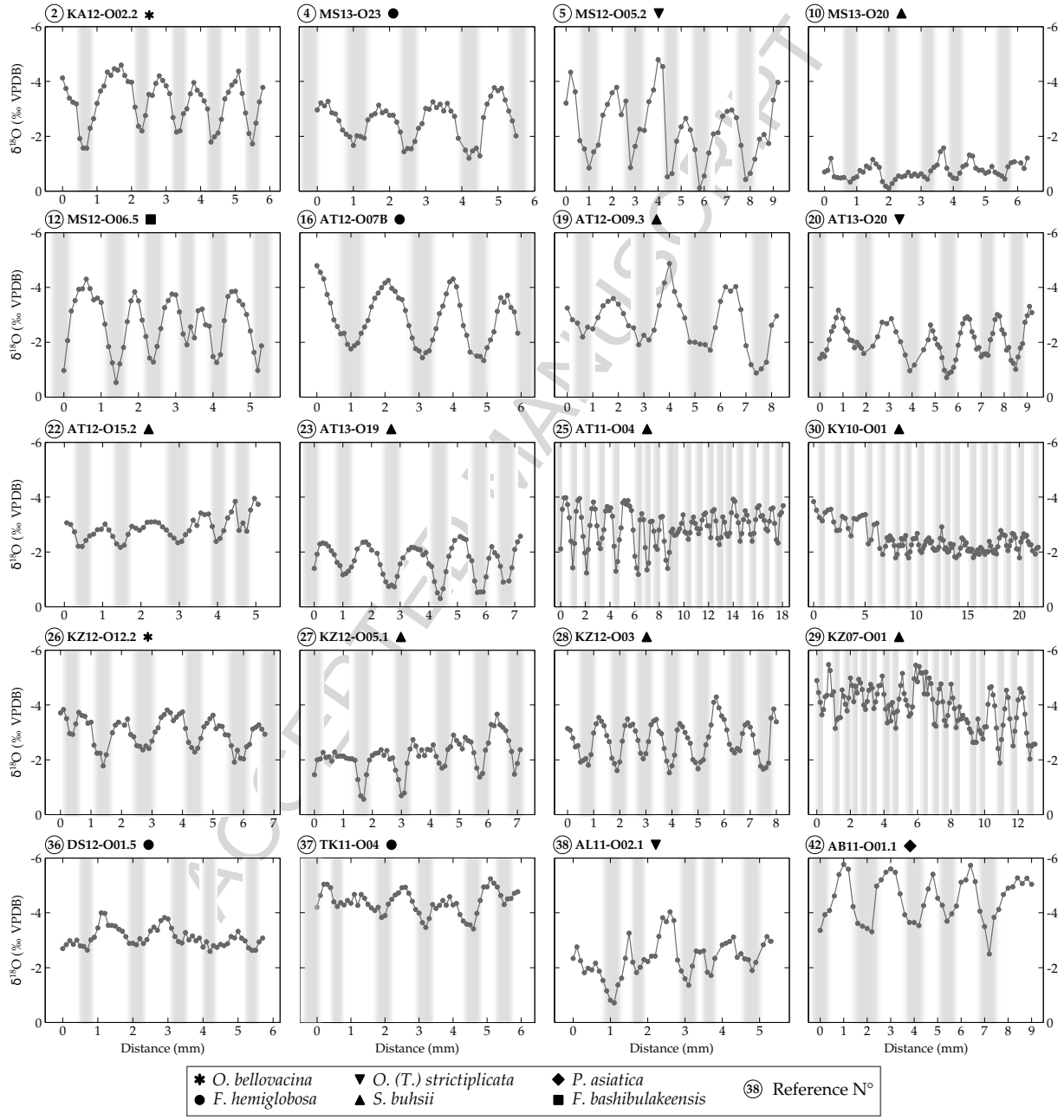

Bougeois et al., 2015
Figure 5

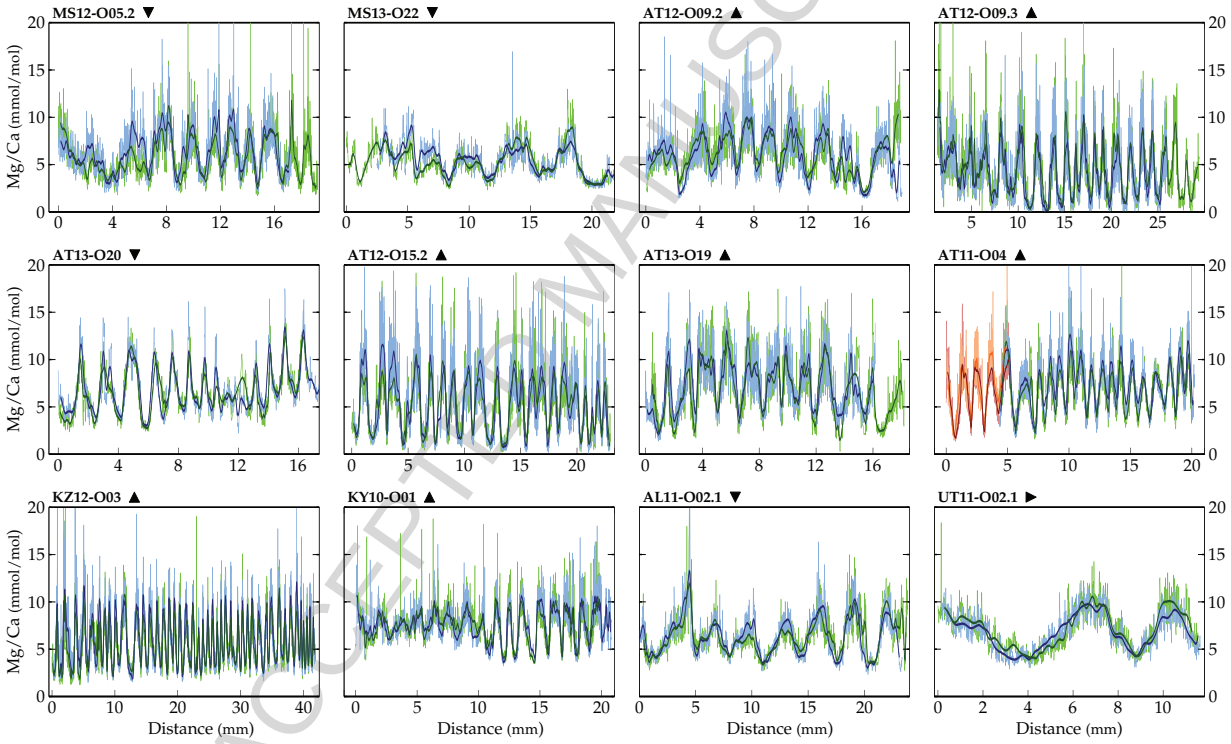

Bougeois et al., 2015
Figure 6

Figure 7

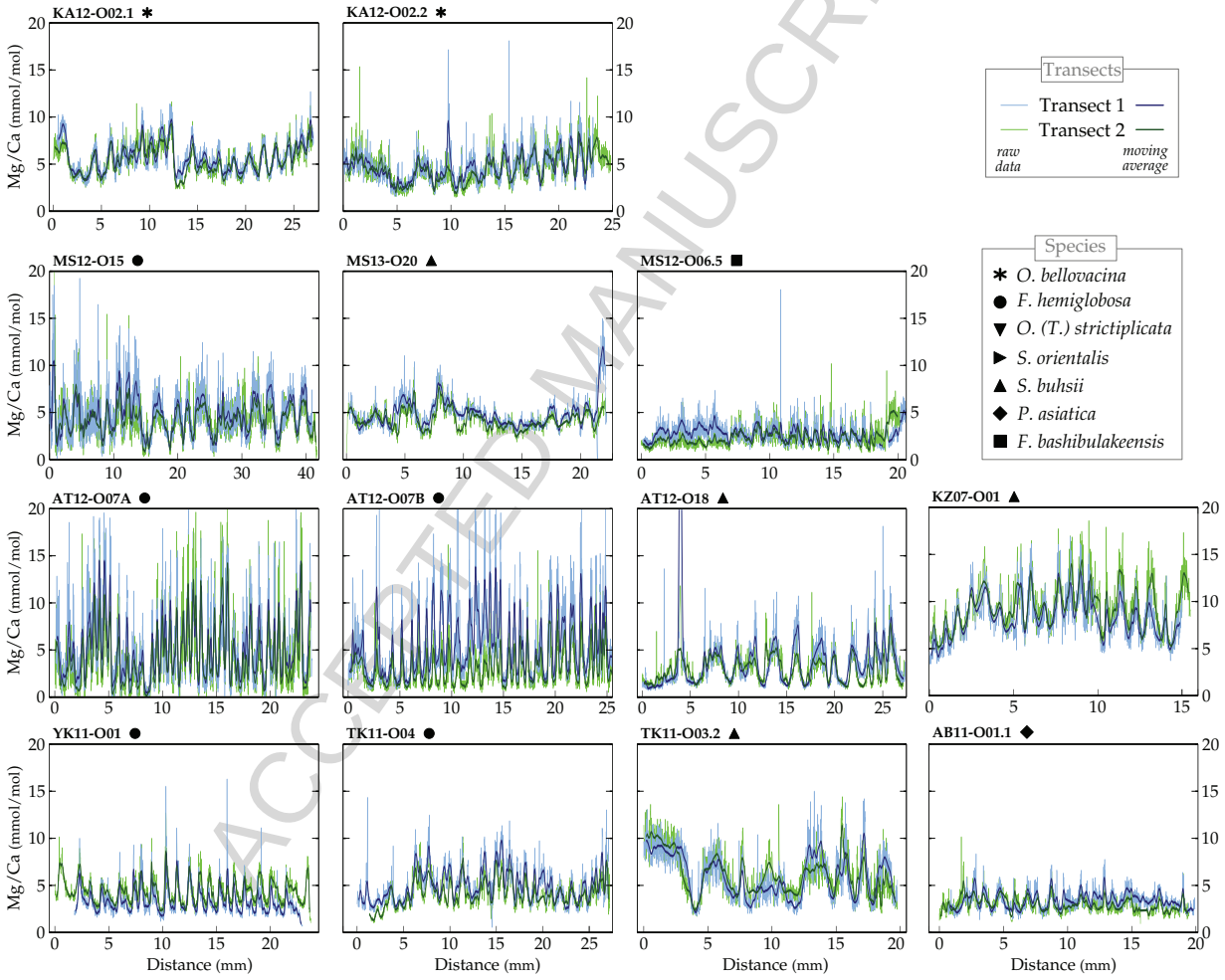

Bougeois et al., 2015
Figure 7

Figure 8

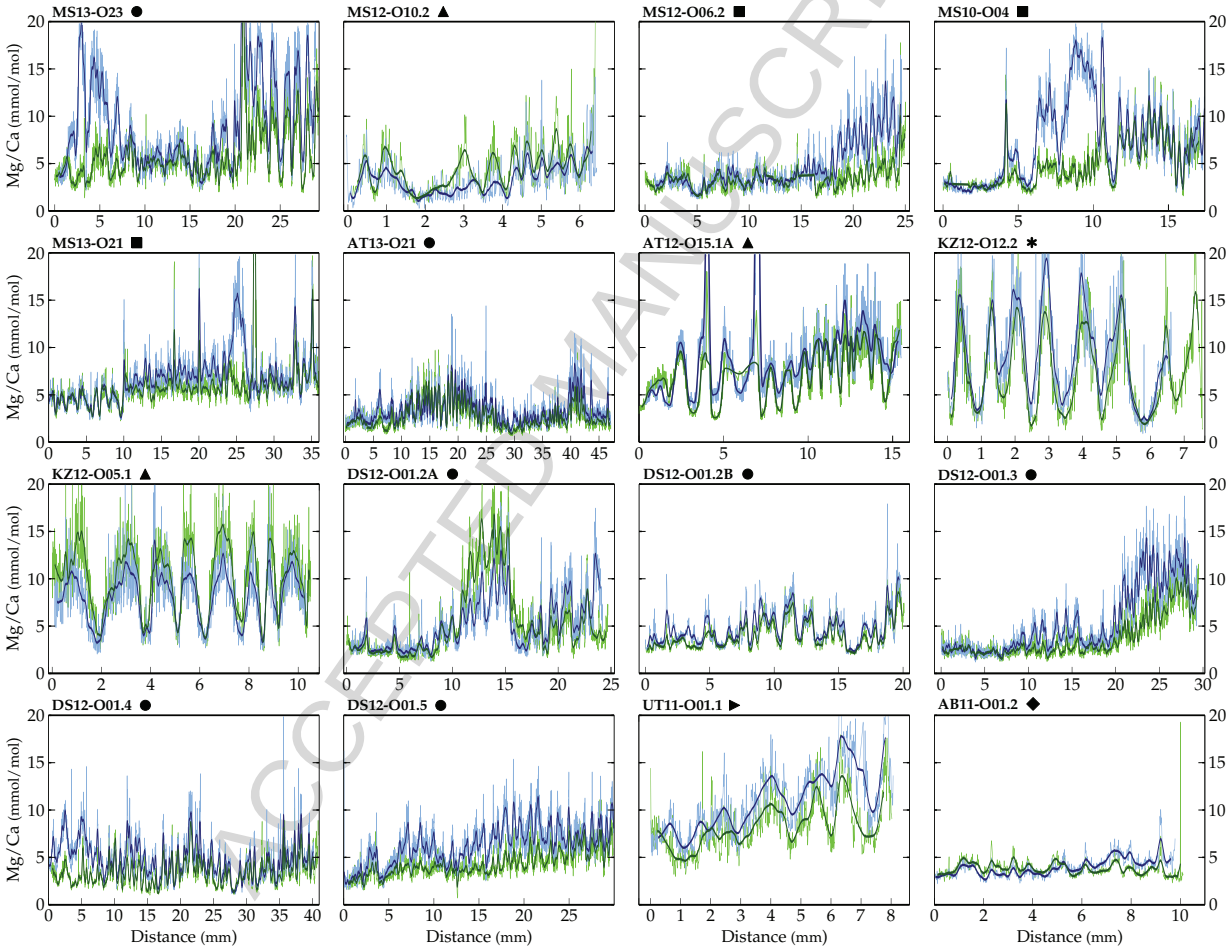

Bougeois et al., 2015
Figure 8

Figure 9

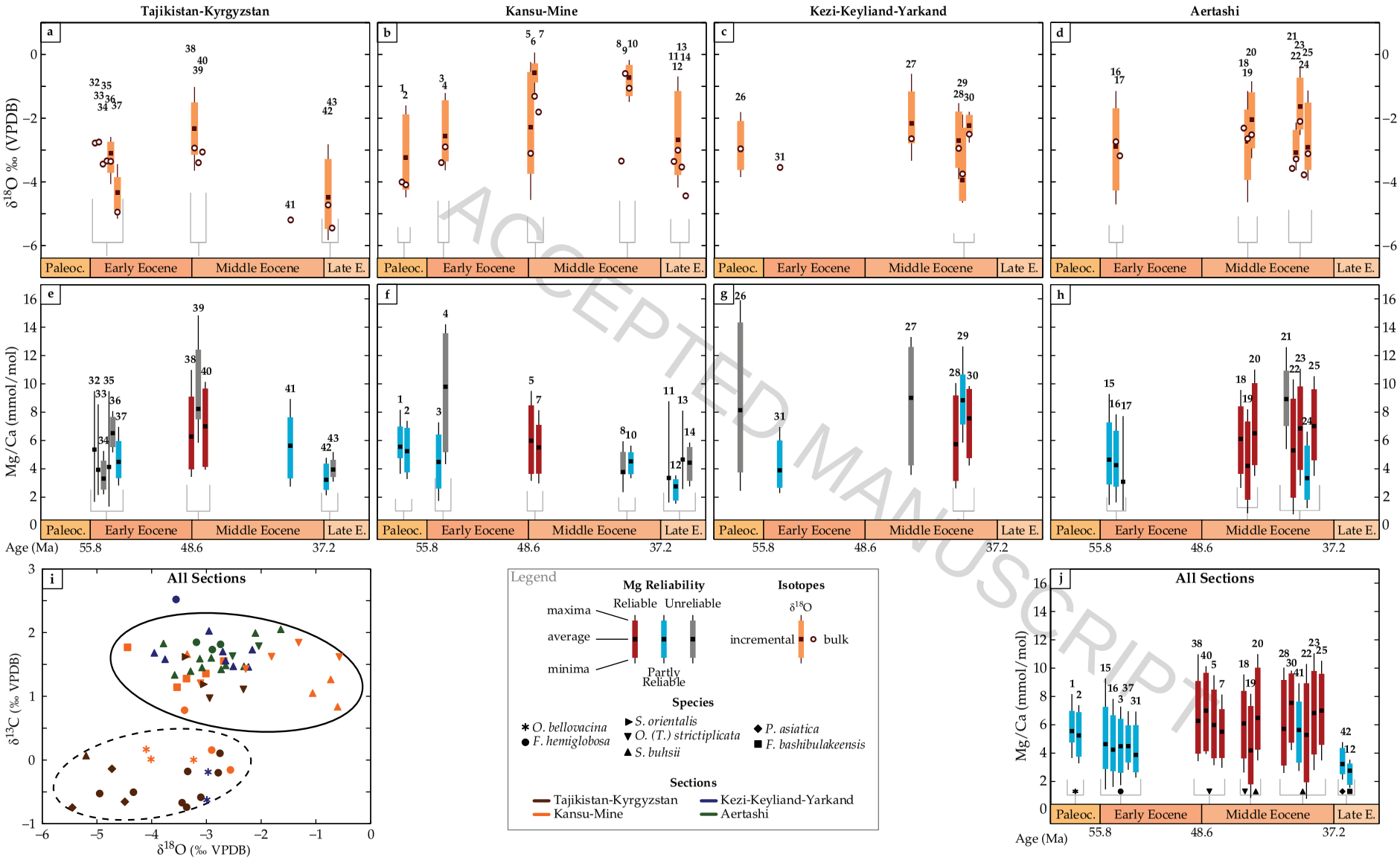

Bougeois et al., 2015
Figure 9

Figure 10

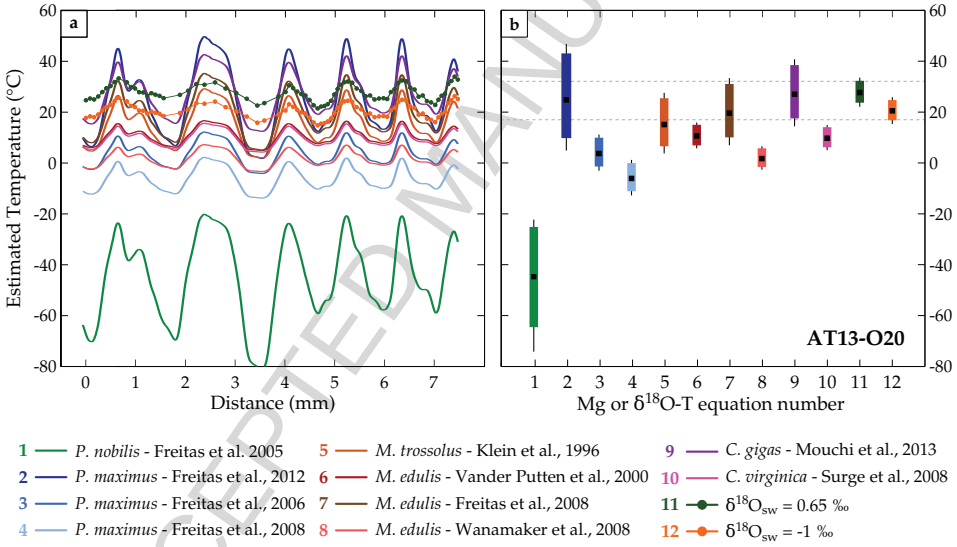

Bougeois et al., 2015
Figure 10

Figure 11

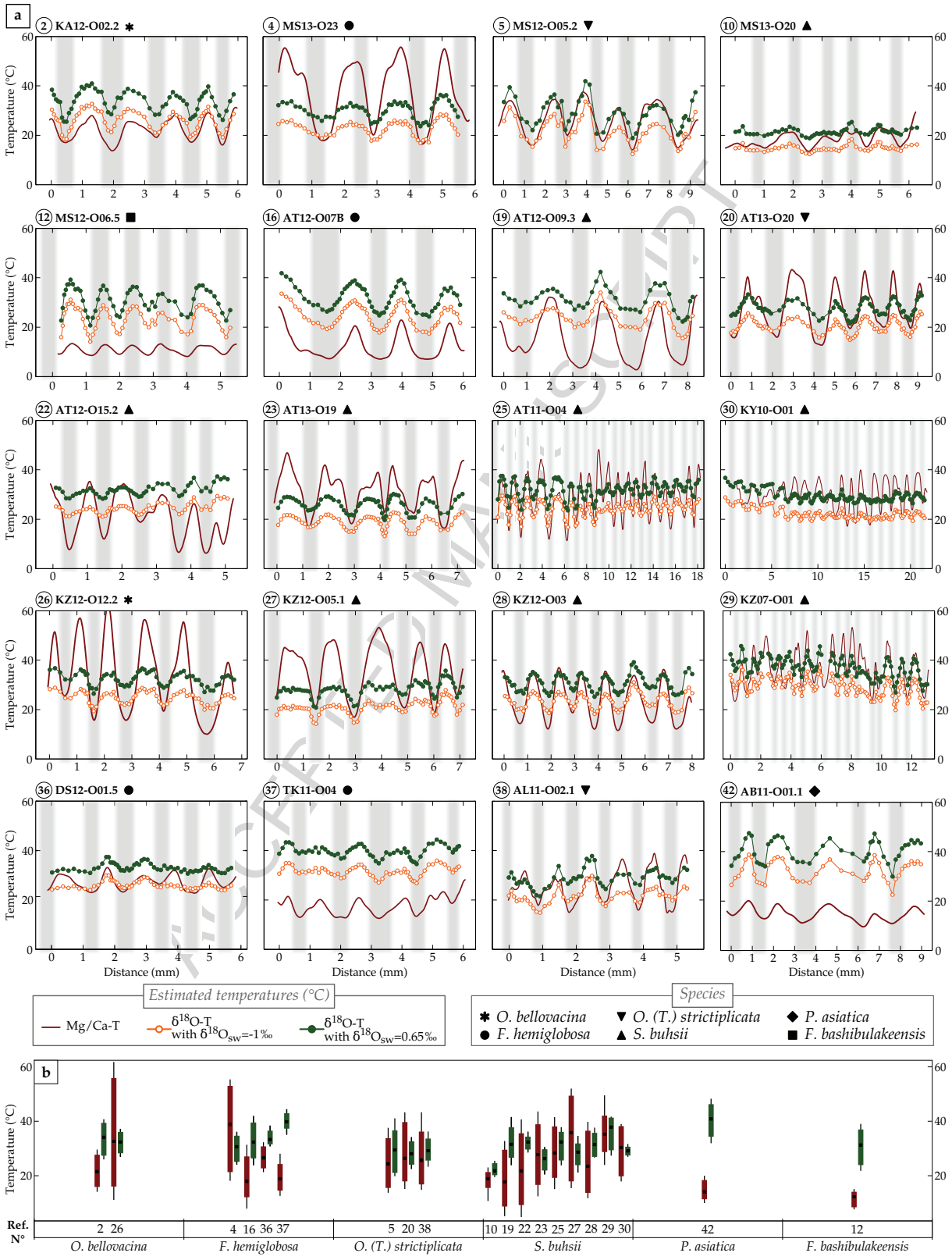

Bougeois et al., 2015
Figure 11

Highlights:

- New application to recover seasonal temperatures from Mg/Ca in fossil oyster shells

- 40 specimens analysed from 7 species living in the Palaeogene Paratethys Sea

- Combining Mg/Ca and δ18O to identify reliable species and salinity variations

- Assessing seasonal temperatures in semi-arid area